


EXPRESS LETTER

Open Access



The first simultaneous spectroscopic and monochromatic imaging observations of short-wavelength infrared aurora of N_2^+ Meinel (0,0) band at $1.1 \mu\text{m}$ with incoherent scatter radar

Takanori Nishiyama^{1,2*} , Masato Kagitani³, Senri Furutachi⁴, Yuki Iwasa⁵, Yasunobu Ogawa^{1,2}, Takuo T. Tsuda⁴, Peter Dalin⁶, Fuminori Tsuchiya³, Satonori Nozawa⁷ and Fred Sigernes⁸

Abstract

This study presents a first simultaneous observation of N_2^+ Meinel (0,0) band (hereafter, N_2^+ (M)) aurora by cutting-edge short-wavelength infrared imaging spectrograph (NIRAS-2) and monochromatic camera (NIRAC) installed at the Kjell Henriksen Observatory (78°N, 16°E). On January 21 2023, N_2^+ (M) intensification that is associated with a band-shape aurora structure was observed by the NIRAS-2 and the NIRAC having temporal resolutions of 30 s and 20 s, respectively. In addition, the European incoherent scatter Svalbard Radar also observed electron density variations at the same time. Electron density measured at altitude range from 100 km 120 km shows similar variations as of N_2^+ (M) intensity, which implies that a primary source of N_2^+ (M) emissions is direct collisions of N_2 by precipitating electrons penetrating down to around 100 km altitude (up to 10 keV). However, the observation also demonstrated moderate correlations between N_2^+ (M) intensity and electron density above 140 km, which implies that different N_2^+ (M) generation process, N_2 charge exchange with O^+ , may work up to near 160 km and make a non-negligible contribution to N_2^+ (M) emissions. This hypothesis would be verified with further radar observations or stereo imaging observations useful to estimate the vertical distribution of the emission layers. The N_2^+ (M) is a very promising target wavelength for aurora observation because the quality of sensors is highly expected to improve further and further. Continuous observations with our new instruments will undoubtedly provide an important information of N_2^+ (M) characteristics, for future missions of both balloon-borne and satellite-borne imaging.

Keywords Aurora, Short-wavelength infrared, Ground-based spectroscopic observations, Ground-based imaging, Indium gallium arsenide, Polar cap, Incoherent scatter radar, Kjell Henriksen Observatory

*Correspondence:

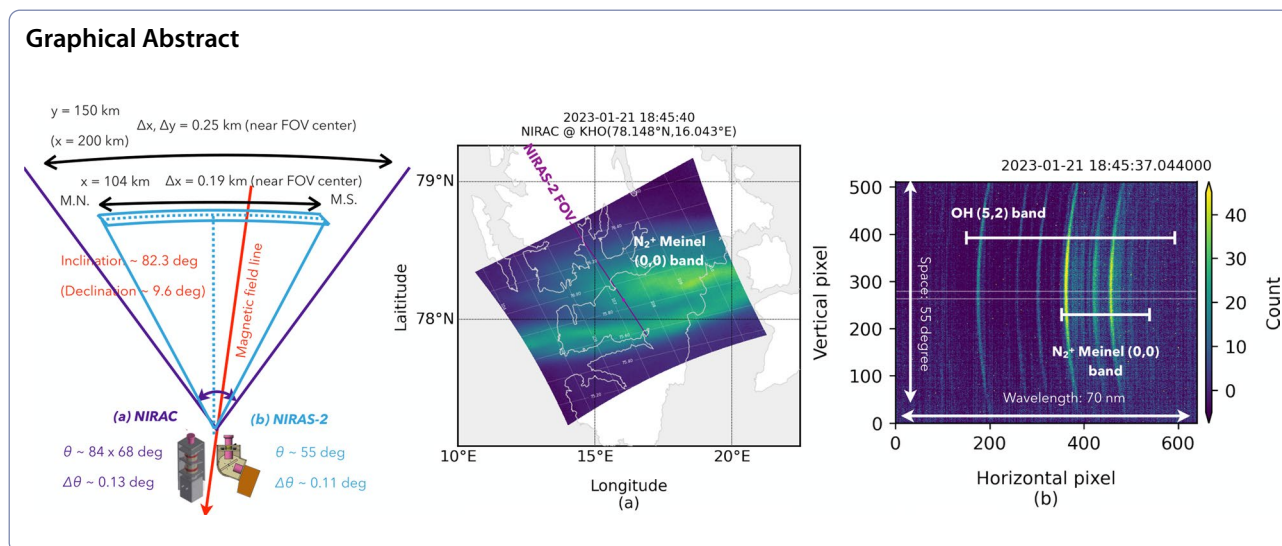
Takanori Nishiyama

nishiyama.takanori@nipr.ac.jp

Full list of author information is available at the end of the article



© The Author(s) 2024, corrected publication 2024. **Open Access** This article is licensed under a Creative Commons Attribution 4.0 International License, which permits use, sharing, adaptation, distribution and reproduction in any medium or format, as long as you give appropriate credit to the original author(s) and the source, provide a link to the Creative Commons licence, and indicate if changes were made. The images or other third party material in this article are included in the article's Creative Commons licence, unless indicated otherwise in a credit line to the material. If material is not included in the article's Creative Commons licence and your intended use is not permitted by statutory regulation or exceeds the permitted use, you will need to obtain permission directly from the copyright holder. To view a copy of this licence, visit <http://creativecommons.org/licenses/by/4.0/>.



Introduction

Auroral emission bands resulting from transitions between the $A^2\Pi_u$ and $X^2\Sigma_g^+$ states of N_2^+ in near infrared regions have been discovered by Meinel (1951). Following the discovery of this N_2^+ Meinel system, several N_2^+ Meinel bands and N_2 1st positive bands were also found in short-wavelength infrared (SWIR) regions (Harrison and Jones, 1957 and references therein). More detailed spectroscopic investigations in SWIR ($\sim 1.6 \mu\text{m}$) have intensively been done in the 1970s (e.g. Gattinger and Jones 1973; Jones and Gattinger 1976; Gattinger and Jones 1981; Dalin et al. 2015); however, only a few study focusing on SWIR aurora was done after Remick et al. (2001). In contrast, SWIR measurements of hydroxyl (OH) airglow have been active over the past decade because of recent advances in indium gallium arsenide (InGaAs) focal plane array (FPA). It enables to measure OH (3,1) band at $1.5 \mu\text{m}$ with high temporal resolutions by a 1-D imaging spectrograph (Schmidt et al. 2013; Singh et al. 2023) and a monochromatic imager with narrow full-width at half-maximum (FWHM) optical filters (Pautet et al. 2014).

Zhou et al. (2007) proposed to take images of sunlit aurora continuously using a monochromatic N_2^+ Meinel (0,0) band camera mounted on a scientific balloon flying at upper stratospheric altitudes. They also did test observations of a panchromatic InGaAs camera in twilight from the ground, and succeeded in taking auroral structures in a slant view. More recently, Nishiyama et al. (2021) reported detailed spectral characteristics in OH Meinel (3,1) band and N_2^+ Meinel band (1,2) measured ground-based 1-D InGaAs spectrograph of Near Infra-Red Aurora and airglow Spectrograph, hereafter NIRAS.

The NIRAS also succeeded updating auroral spectrum from $0.9 \mu\text{m}$ to $1.3 \mu\text{m}$ associated with auroral breakup with a 30-s time resolution (see Additional file 1 in more detail).

However, despite growing its importance, SWIR aurora is less observed so far, and therefore, further investigations are obviously needed for understanding SWIR auroral properties such as generation process, intensity, emission altitude, precipitating electron energy, etc. Simultaneous N_2^+ Meinel (0,0) band and incoherent scatter radar observations have never been done. This is why typical center altitudes of N_2^+ Meinel (0,0) band emission layer were mainly speculative based on only optical measurements, and therefore, the generation process of N_2^+ in the state $A^2\Pi_u$ is still under debate. In addition, since N_2^+ Meinel (0,0) band is thought to be not affected by resonant scattering from N_2^+ uplifted to the upper ionosphere (Remick et al. 2001), pure auroral emissions in N_2^+ Meinel (0,0) band can be measured from the ground in twilight/sunlit time when N_2^+ in the upper ionosphere are illuminated by solar radiations. This is important especially for high-latitude regions, where twilight hours are longer than at mid and low latitudes. In accordance with this scientific background, two cutting-edge optical instruments have been developed to further elucidate SWIR aurora: Near InfraRed Aurora and airglow Spectrograph-2 (NIRAS-2) and Near InfraRed Aurora and airglow Camera (NIRAC). Ground-based observations with the new two instruments have been initiated at the Kjell Henriksen Observatory (KHO), Longyearbyen (78.1°N , 16.0°E) since November 2022 to study magnetosphere–ionosphere–atmosphere coupling processes in the high polar regions. In this paper, initial results based

on simultaneous observations of the two instruments and the European incoherent scatter Svalbard Radar (ESR) are presented.

Instruments

The NIRAS-2 is a brand-new SWIR imaging spectrograph designed for the wavelength range from 1.05 to 1.35 μm in which sky background intensity is weaker than in visible subrange. It targets on strong auroral emissions such as the N_2^+ Meinel (0,0) band (hereafter, N_2^+ (M)) and the N_2 1st Positive bands (0,0, and 0,1) as well as on the airglow of OH Meinel bands. The NIRAS-2 is composed of three SWIR lenses, three slits (30-, 60-, and 90- μm), two volume phase holographic gratings (VPHGs) (950 lpmm and 1500 lpmm), an optical filter to remove higher order diffraction light, and 2-D InGaAs FPA. Different types of slits and VPHGs can be switched by actuators, and therefore, wavelength and spectral resolution of the observation target can be changed remotely. If the high-dispersion grating is used (called aurora fine mode), spectral bandpass are 0.21 nm and 0.44 nm with the 30- and 60- μm slits, respectively. Its field-of-view (FOV) and angular resolution are 55 degrees and 0.11 degrees per pixel.

The NIRAS measures only at single point along the magnetic field line and is equipped with an InGaAs FPA with relatively large dark noise ($-52\pm 0.2^\circ\text{C}$). On the other

hand, the NIRAS-2 has one-dimensional FOV and, is characterized as low and stable dark noise of the InGaAs FPA due to 4-stage peltier cooling system ($-80\pm 0.01^\circ\text{C}$). The former allows us to distinguish spatial and temporal changes in highly variable aurora phenomena along the meridional direction. As a result, auroral arc structures with meridional width as narrow as few degrees can be spatially resolved. The latter is important especially for analysis of airglow emissions. The main target of the NIRAS-2 airglow observations is the OH Meinel bands from 1.05 to 1.35 μm that are relatively weak compared to the OH (3,1) band. The NIRAS-2 can not only measure the OH bands intensities with enough quality but it also estimates OH rotational temperature, which has been difficult to perform with the NIRAS.

In addition to the NIRAS-2, a brand-new SWIR imager, NIRAC, has been developed focusing on aurora emissions in N_2^+ (M). The N_2^+ (M) is about two orders brighter than the N_2^+ 1st negative band at 427.8 nm (Remick et al. 2001), which means that the band can be a good indicator of energetic electron precipitations. The imager consists of a few commercial SWIR lenses that are typically used for security/defense purposes, plano-convex lenses, a custom optical filter (center: 1113 nm, FWHM: 13.8 nm) and a 2-D InGaAs FPA. Total optical system is fast (F -number 1.5) and its meridional coverage of the NIRAS-2 ($84^\circ \times 68^\circ$) is slightly wider than the meridional coverage of the NIRAS-2. NIRAC can visualize two-dimensional structures of not only aurora but also even weak OH airglow with a cadence of less than 30 s. Thus, the NIRAC is used as a twin instrument to the NIRAS-2 to help in interpreting meridional scan data obtained from the NIRAS-2. Detailed specifications of the both optical instruments are shown in Table 1.

Absolute sensitivity of both the instruments was calibrated by light sources consists of two integrated spheres with different diameters (76-inch and 6-inch) and different lamps in the following two steps. At first, using spatially uniform light, which is traceable to the spectral irradiance standard of National Metrology Institute of Japan, emitted from a port (diameter less than 20 mm) of the small integrated sphere, absolute sensitivity was calibrated only in the centers of the FOVs. Next, light from the large integrate sphere, which can illuminate the whole FOVs, was used to calibration for non-uniform sensitivity within the FOVs caused by each optical system.

FOV calibration of the NIRAC was performed by estimating positions of reference stars. The camera optical model was chosen as the third-order polynomial. By comparing theoretical horizontal coordinates of reference stars with their measured coordinates, ten coefficients of the third-order polynomial were calculated. These ten coefficients describe all possible optical

Table 1 Key properties of the NIRAS-2 and the NIRAC

Specifications of the NIRAS-2	
Field-of-view	$0.11^\circ \times 55^\circ$ (Meridional direction)
Spatial resolutions	0.11° , 0.19 km near the center of the FOV
Time resolutions	30 seconds
2-D FPA	640×512 pixels, 15- μm pixel size, -80.0°C
Aurora fine mode ^a	
Spectral resolutions (FWHM)	0.21/0.44 nm with 30-/60- μm slit
Wavelength range	1065–1135 nm
Target emissions	N_2^+ Meinel (0,0) (and OH Meinel (5,2))
Specifications of the NIRAC	
Field-of-view	$84^\circ \times 68^\circ$
Spatial resolutions	0.13° , 0.25 km near the center of the FOV
Time resolutions	15 or 20 or 30 sec
Filter center wavelength	1113 nm
Filter width (FWHM)	13.8 nm
2-D FPA	640×512 pixels, 20- μm pixel size, -55.0°C
Target emissions	N_2^+ Meinel (0,0) and OH Meinel (5,2)

^a Other three modes with different targets and resolutions are also available

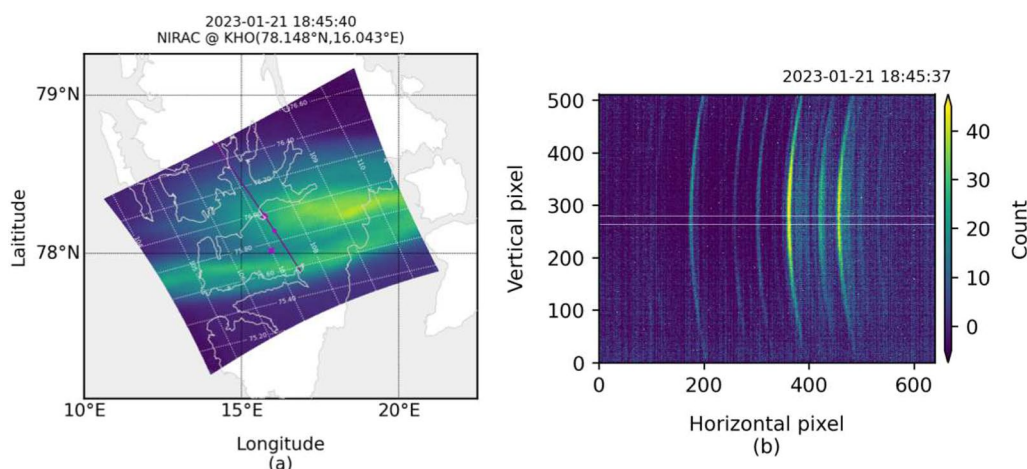


Fig. 1 **a** An image of a band-shaped aurora obtained by the NIRAC. It is mapped onto geographical coordinates at 110 km altitude. White dotted lines on the image are Altitude-Adjusted Corrected GeoMagnetic (AACGM) latitude and longitude (Shepherd 2014). A darkmagenta line indicates the FOV of the NIRAS-2, and darkmagenta circle, diamond, cross are the positions of the KHO, the NIRAS-2 data of interest in subsequent analyses, and the ESR beam. **b** A dark-subtracted image obtained by the NIRAS-2 when the band-shaped aurora appeared. Horizontal and Vertical axes correspond to wavelength and space (meridional), respectively

distortions in the whole camera optical path. Then the georeference procedure, projecting each pixel of the sensor on the Earth's surface, was done assuming the mean N_2^+ (M) emission altitude of 110 km. Detailed information on the optical calibration, georeference procedure and error analysis can be found in Dalin et al. (2015). The NIRAS-2 has captured many dark frames in different modes and at different exposure times previously in a laboratory. For the NIRAC, six dark frames are taken automatically before doing every daily observation.

In addition with such optical instruments, a result of a special experiment for the ESR requested by the United Kingdom on January 21, 2023 is demonstrated. In the experiment, only a 42-m antenna radar aligned along the direction of the local geomagnetic field (elevation 82.3° and azimuth 189.6°) was in operation. The FOV of the NIRAC covers the local magnetic zenith, but the one of the NIRAS-2 does not. This is because it is approximately along the magnetic meridian and rotated by -25° in the azimuthal direction.

Results

One event in which intensification of N_2^+ (M) was observed by the NIRAS-2 and the NIRAC on January 21, 2023 is reported. This was the first ever simultaneous spectral and monochromatic imaging of N_2^+ (M) from the ground. In addition, the ESR also observed ionospheric variations associated with the auroral activity at the same time. Figure 1 shows (a) an aurora image taken by the NIRAC with 20-s exposures that is mapped onto geographical coordinate at 110-km altitude and

(b) a dark-subtracted image of aurora spectrum in format of wavelength (horizontal) and space (vertical) axes taken by the NIRAS-2 with 30-s exposures. In Fig. 1(a), a darkmagenta line indicates the FOV of the NIRAS-2, and darkmagenta circle, diamond, and cross are the positions of the KHO, the NIRAS-2 data of interest in subsequent analyses, and the ESR beam. The NIRAC shows a banded-shape structure with a peak intensity is 35 kR and the intensity corresponding to the position of the magenta diamond is about 30 kR. More detailed temporal and spatial variability of the aurora event can be seen in Additional file 2 that is a NIRAC movie for 24 h starting from local noon on the date. Enhanced aurora spectrum of N_2^+ (M) can be seen in between pixels 380 (1103 nm) to 500 (1120 nm) along the wavelength axis. Figure 2 shows the corresponding spectral lines for a region surrounded by the white region in Fig. 1(b).

Figure 2(a) shows 10-min averaged spectrum as reference of background made from ones taken before beginning of the aurora activity (blue) and taken at the peak intensification (orange), respectively. Nominal aurora spectrum, which is created by subtracting the reference from the spectrum of interest, is a red line plot in Figure 2b. Three peaks related to N_2^+ rotational motion are clearly seen with a spectral resolution of 0.44 nm. Absolute intensity integrated between 1103 and 1120 nm (indicated by red vertical lines) is estimated to be about 50.0 kR. On the other hand, a green line plot is convolution of the nominal aurora spectrum and the NIRAC filter function. It demonstrates that the NIRAC can capture the most part of N_2^+ (M) spectrum. Absolute intensity

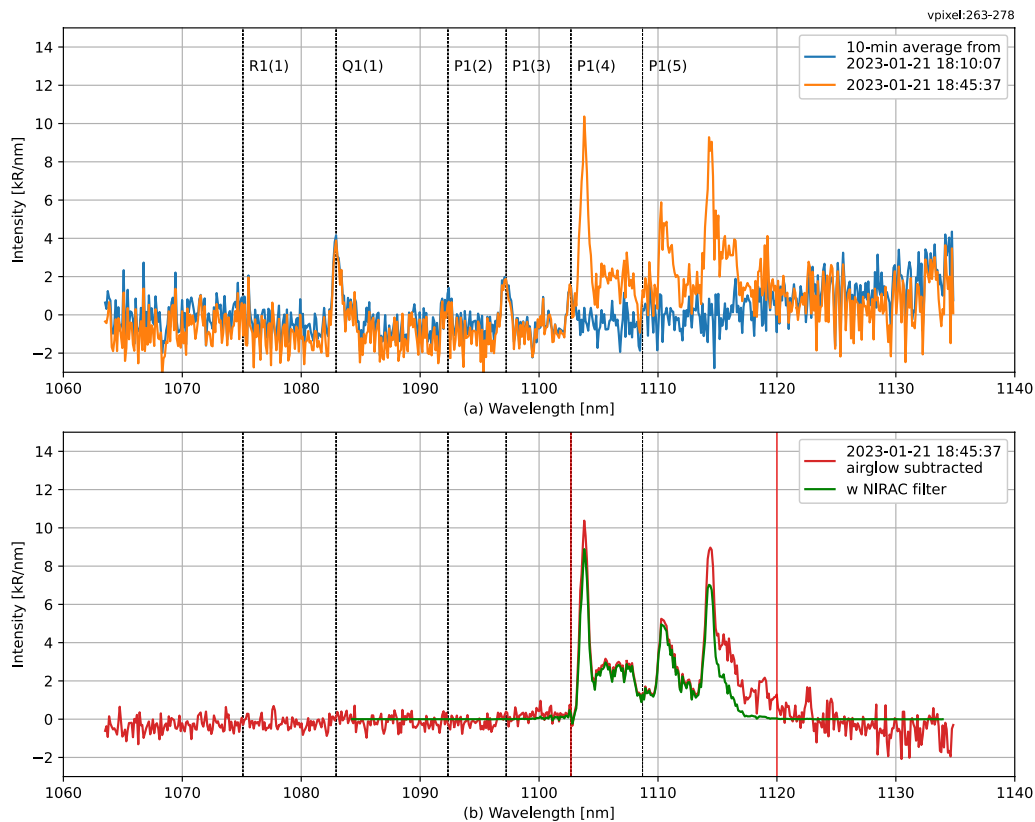


Fig. 2 **a** 10 min averaged spectrum taken before the aurora intensification (blue) and spectrum taken at the peak of the aurora intensification (orange). **b** Nominal aurora spectrum (red, see details in the text) and spectrum created from convolutions of the observed $N_2^+(M)$ spectrum and the NIRAC filter transmittance functions (green)

with the NIRAC filter is 38.6 kR, which is roughly consistent with the NIRAC measurements.

Focusing on time evolution of $N_2^+(M)$, a summary plot with a ground-based magnetometer at Longyearbyen and the ESR is shown in Fig. 3. $N_2^+(M)$ intensity was enhanced twice between 18:20 and 18:55 UT (b and c) synchronized with the observed H-component depletions (a). But, interestingly, the latter highest peak of $N_2^+(M)$ was seen with a shallow depletion of the H-component. Figure 3b demonstrates the $N_2^+(M)$ intensity observed by the NIRAS-2 and the NIRAC showing similar time variations with a high positive correlation coefficient of 0.90. Although the NIRAC underestimated the $N_2^+(M)$ intensity especially when the intensity became larger, the difference is still acceptable taking account into the NIRAC filter and optical dome transmittance. This is discussed below in more detail. Figure 3d shows electron density variations along the field line with 30-s cadence from 80 to 300 km altitude observed by the ESR. During the same period, strong ionizations down to 90-km altitude occurred twice as well. Figure 3e shows electron density

variations at specific altitudes (81, 97, 114, and 142 km) along the field line. Electron densities changed at these altitudes roughly in the same way as $N_2^+(M)$ intensity, but the change is not clear at the lowest altitude. With regard to 142 km altitudes, electron density still kept high even after $N_2^+(M)$ intensity decreased, which implies that $N_2^+(M)$ is effectively generated by electron precipitations penetrating down to around 100 km altitude.

More detailed comparisons between $N_2^+(M)$ intensity and electron density at different altitudes for the time interval from 18:20:07 to 18:54:07 are presented in Fig. 4. Figure 4a displays scatter plots for $N_2^+(M)$ intensity observed by the NIRAS-2 versus electron density observed at 85–200 km altitudes, showing that the electron density is higher with increasing $N_2^+(M)$ intensity. If ionization rate is proportional to square of electron density, which is true if electron density can be regarded as a steady state in the E region, then it would be expected that volume emission rate of $N_2^+(M)$ has the same relationship with electron density. Figure 4b is correlation between the $N_2^+(M)$

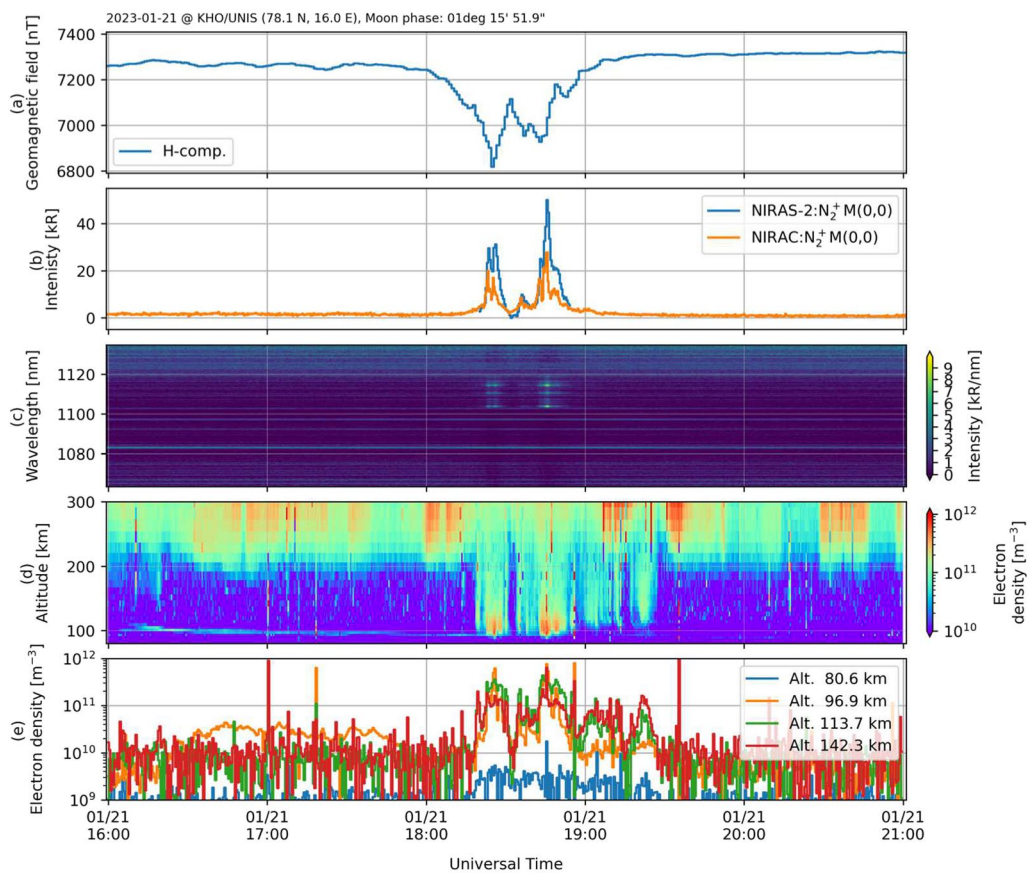


Fig. 3 Summary plots for temporal evolution of the observed $N_2^+(M)$ with ionospheric variations. **a** H-component of geomagnetic fields, **b** $N_2^+(M)$ intensity observed by the NIRAS-2 and the NIRAC, **c** dynamic spectrum from 1065 to 1135 nm obtained by the NIRAS-2, **d** electron density along the filed line as functions of altitude and time, and **e** electron density variations for the four different altitudes along the filed line observed by the ESR

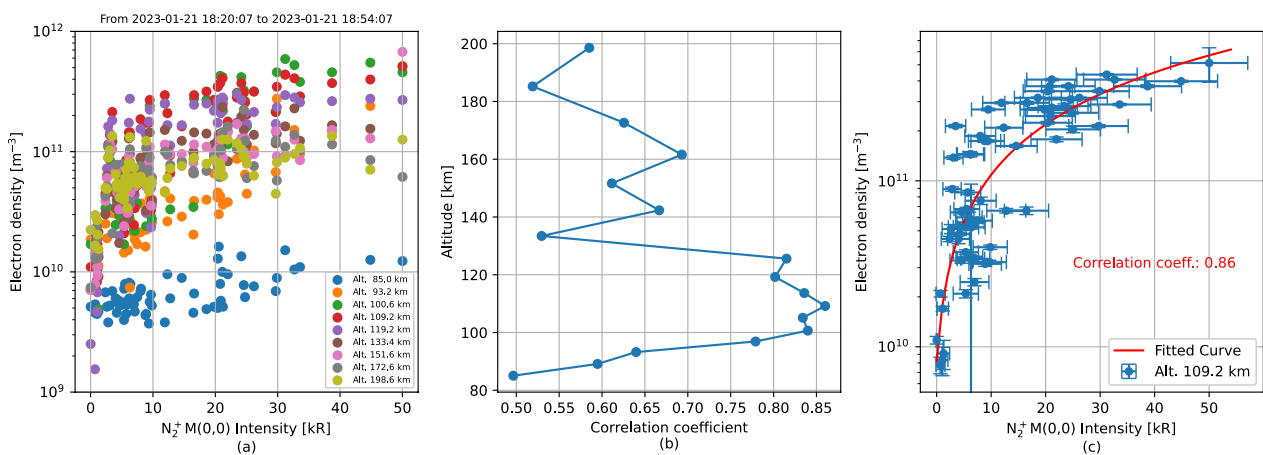


Fig. 4 **a** Scatter plots for $N_2^+(M)$ intensity observed by the NIRAS-2 and electron density for different altitudes. **b** Correlation coefficients between the $N_2^+(M)$ intensity and the squared electron density as a function of altitudes. **c** A scatter plot for 110 km altitude in the same format as **a**. A red line is a fitted curve for the assumption that $N_2^+(M)$ intensity is proportional to the squared electron density

intensity and the squared electron density as a function of altitudes from 85 to 200 km. The correlation is high in altitude range from 100 to 120 km with a peak at 110 km and the highest correlation coefficient of 0.86. The correlation drops sharply near 130 km, and a sub-peak is also found at 162 km. It may be due to different production mechanism playing a role at different altitudes for the production of N_2^+ (M) emission. Figure 4(c) is the same plot as (a) but for the altitude of 110 km. A red line is a fitted curve assuming that N_2^+ (M) intensity is proportional to squared electron density and it shows a good agreement with the observation. Therefore, the assumption, N_2^+ (M) is mainly generated by direct electron impacts and its intensity is proportional to squared electron density, is established well at the altitude. This is examined not only by the NIRAS-2 measurements (Corr. coeff., 0.86) but also by the NIRAC measurements (Corr. coeff., 0.72).

Discussion and conclusions

The first ever simultaneous spectroscopic and imaging observations of N_2^+ Meinel (0,0) band at KHO on January 21, 2023 are presented. The former was done by the wide FOV imaging spectrograph with a 30-s cadence and a spectral resolution of 0.44 nm. The latter was successfully done as the first monochromatic imaging of N_2^+ (M) aurora structures so far. The auroral intensities of N_2^+ (M) measured by the both instruments show some agreement: 38 kR and 30 kR by the NIRAS-2 and the NIRAC, respectively. The intensity by the NIRAS-2 is 1.3 times greater than by the NIRAC. Possible reasons for this discrepancy include differences in the time resolution and timing of the respective measurements, but further investigation is needed. N_2^+ (M) system has multiple lines in 1103–1134 nm range, and those at wavelength shorter than 1120 nm mainly contributed to total intensity of N_2^+ (M) as shown in Fig. 2. Intensity of the lines at longer wavelength is minor, and it is difficult to measure from the ground since they should be greatly absorbed by water vapor in the troposphere. A part of P-branch in OH (5,2) band also exists in the wavelength range, but typical their intensity is up to 3 kR, which is not significant with respect to the N_2^+ (M) intensity. Therefore, measurement of N_2^+ (M) up to 1120 nm is one of the key ways of gaining signal-to-noise ratio especially for monochromatic imaging.

This case study shows the first simultaneous optical N_2^+ (M) observation and incoherent scatter radar observation. Generation processes of N_2^+ (M) are poorly understood partly due to the lack of simultaneous ionospheric observations. Previous studies have suggested that direct electron impact plays a dominant role in production of N_2^+ ($A^2\Pi_u$) (Jones and Gattinger 1976; Gattinger and

Jones 1981; Remick et al. 2001). Based on the ESR observation, N_2^+ (M) intensity correlates with squared electron density at 100–120 km very well. This is consistent with that a primary source of N_2^+ (M) emissions is direct collisions of N_2 by precipitating electrons (up to 10 keV). However, the result also suggests that N_2^+ (M) generation process worked at the same time near 160 km. A plausible candidate is charge exchange with O^+ (Omholt 1957), which is expected to occur at higher altitude (> 120 km) (Dalín et al. 2015). The charge exchange is believed to effectively produce N_2^+ ($A^2\Pi_u, v' = 1$) rather than N_2^+ ($A^2\Pi_u, v' = 0$), but this process may make a non-negligible contribution to N_2^+ (M) emissions. This hypothesis would be verified with further radar observations or stereo imaging observations useful to estimate the vertical distribution of emission layers. Although the ESR demonstrated that continuous ionizations above 120 km probably associated by soft electron precipitations after 19 UT, no any increases in N_2^+ (M) intensity are seen during the period. This implies that for $N_2 - O^+$ charge exchange to be efficient energetic electron precipitations must be required as well.

Although further improvements will be applied to our system, it can be concluded that one method of ground-based auroral observation in SWIR has been established and verified. N_2^+ (M) is a very promising target wavelength for aurora observation because the quality of InGaAs FPA is highly expected to improve further and further. Since N_2^+ (M) intensity for International Brightness Coefficient III aurora is estimated 160 kR (Gattinger and Jones 1981), such bright aurora events enable us to measure with high spectral resolutions and/or high temporal resolutions. In addition, sky background intensity is weaker in SWIR than in visible subrange. Spectroscopic observations with higher spectral resolutions are effective in to suppress sky background intensity, which may allow us to more twilight/daytime aurora measurements even from the ground as was done in visible subrange (e.g. Rees et al. 2000; Pallamraju and Chakrabarti 2005). Another important aspect of N_2^+ (M) is that it is considered as a target wavelength for sunlit auroral observations from stratospheric balloons (Zhou et al. 2020). Continuous observations based on the new ground-based instruments will undoubtedly provide an important feature of N_2^+ (M), both for balloon-based observations and for future satellite-borne imaging missions.

Abbreviations

SWIR	Short-wavelength infrared
OH	Hydroxyl
InGaAs	Indium gallium arsenide
FPA	Focal plane array
FWHM	Full-width at half-maximum
NIRAS	Near InfraRed Aurora and airglow Spectrograph

NIRAS-2	Near InfraRed Aurora and airglow Spectrograph-2
NIRAC	Near InfraRed Aurora and airglow Camera
KHO	Kjell Henriksen observatory
ESR	European incoherent scatter Svalbard radar
$N_2^+(M)$	N_2^+ Meinel (0,0) band
VPHG	Volume phase holographic grating
FOV	Filed of view
AACGM	Altitude-adjusted corrected geomagnetic coordinates

Supplementary Information

The online version contains supplementary material available at <https://doi.org/10.1186/s40623-024-01969-x>.

Additional file 1: SWIR aurora and airglow spectrum observed by the NIRAS on May 8, 2018. This spectrum is obtained from the NIRAS working at Syowa station, Antarctica in 2018, and a spectral resolution is about 1.9 nm. Top and bottom panels show spectrum from 0.9 to 1.15 and those from 1.00 to 1.30 μm , taken at the same night. Black lines are nightly mean spectrum that can be regard as background OH and airglow spectrum. Red and blue lines are nominal aurora spectrum with 2.5 min and 30 s resolutions, corresponding to aurora intensification at 01:54:00 UT, May 9, 2018. Many auroral emissions such as N_2^+ Meinel bands (v', v'') = (1,0), (2,1), and (0,0) and N_2 1st positive bands (v', v'') = (0,0) and (0,1) are recognized.

Additional file 2: An NIRAC movie on January 21, 2023. This movie is created from the NIRAC images with 20-sec cadence. Time period of this movie is 24 h, starting from local noon on the date. A color scale ranges from 0 kR to 30 kR. White dotted lines in the image correspond to latitude and longitude calculated by AACGM version 2. The symbols indicate the same positions as shown in Fig. 1(a). Sky was covered with clouds in the most of the period; however, drastic changes in $N_2^+(M)$ auroral intensity and structure can be seen during the period from 18 to 19 UT.

Acknowledgements

The corresponding author appreciates Dr. Mikko Syrjäsoo so much for his continuous and dedicated support for the installation and operation of our instruments. Dr. Daniel Whiter has kindly shared the ESR data presented in this study with us, and the corresponding author would like to sincerely acknowledge him. This study and observation were supported by the joint research program of Planetary Plasma and Atmospheric Research Center, Tohoku University, the joint research program of the Institute for Space-Earth Environmental Research, Nagoya University and the Project Research KP301 of the National Institute of Polar Research. Ground-based fluxgate data access and processing was done using pyspedas v1.4.28, see Angelopoulos et al. (2019).

Author contributions

TN (corr-auth) designed this research, installed and operated the NIRAS-2 and the NIRAC at KHO, led data analysis, and wrote the first draft of manuscript. MK and TN developed the NIRAS-2 and the NIRAC. TN, MK, SF, YI, and TT contributed integrations of NIRAS-2 and NIRAC system and discussed analysis method. PD contributed analysis of the NIRAC, optical calibration, and discussion of NIRAC results. YO, SN, and FS contributed NIRAS-2 and NIRAC installation at KHO and support ESR operations. FT was involved in this research and discussions. All authors contributed improving the manuscript. All authors have read and approved the final manuscript.

Funding

The NIRAS-2 and NIRAC were funded by Japan Society for the Promotion of Science (JSPS), Grants-in-Aid for Young Scientists (A) 17H04857, Scientific Research (B) 20H01955, (B) 20H01962, and (B) 21H01144. They were also partly funded by Shimadzu Science Foundation, and Hosono Bunka Foundation Grants.

Availability of data and materials

The NIRAS-2 and NIRAC data can be provided on request basis to Dr. Nishiyama, NIPR. The ESR observation presented in this study has been carried out as a special program led by Dr. Whiter, University of Southampton. The ESR data were used according to EISCAT Data Rules of the Road ("https://eiscat.se/

scientist/data/"). Ground-based fluxgate magnetometer data can be found at "http://themis.ssl.berkeley.edu/data/themis/thg/greenlandmag/12/lyr/2023/".

Declarations

Ethics approval and consent to participate

Not applicable.

Consent for publication

Not applicable.

Competing interests

The authors declare that they have no competing interests.

Author details

¹National Institute of Polar Research, 10-3, Midori-cho, Tachikawa, Tokyo 190-8518, Japan. ²Department of Polar Science, The Graduate University for Advanced Studies, SOKENDAI, 10-3, Midori-cho, Tachikawa, Tokyo 190-8518, Japan. ³Tohoku University, 6-3, Aramaki Aza-Aoba, Aoba-ku, Sendai, Miyagi 980-8578, Japan. ⁴Department of Computer and Network Engineering, University of Electro-Communications, 1-5-1, Chofugaoka, Chofu, Tokyo 182-8585, Japan. ⁵National Metrology Institute of Japan (NMIJ), National Institute of Advanced Industrial Science and Technology (AIST), 1-1-1, Umezono, Tsukuba, Ibaraki 305-8563, Japan. ⁶The Swedish Institute of Space Physics, Box 812, SE-981 28 Kiruna, Sweden. ⁷Institute for Space-Earth Environmental Research, Nagoya University, Furo-cho, Chikusa-ku, Nagoya, Aichi 464-8601, Japan. ⁸University Centre In Svalbard, Longyearbyen, Norway.

Received: 21 June 2023 Accepted: 19 January 2024

Published: 15 February 2024

References

- Angelopoulos V, Cruce P, Drozdov A et al (2019) The space physics environment data analysis system (SPEDAS). *Space Sci Rev* 215:9. <https://doi.org/10.1007/s11214-018-0576-4>
- Espy PJ, Pendleton WR Jr, Sivjee GG, Fetrow MP (1987) Vibrational development of the N_2^+ Meinel Band System in the aurora. *J Geophys Res Space Phys* 92:11257–11261. <https://doi.org/10.1029/JA092iA10p11257>
- Gattinger RL, Jones A, Vallance (1973) N_2^+ Meinel auroral spectra in the 1.5 μm region. *Can J Phys* 53:480–487. <https://doi.org/10.1139/p73-036>
- Gattinger RL, Jones A, Vallance (1981) Quantitative spectroscopy of the aurora. V. the spectrum of strong aurora between 10000 and 16000 Å. *Can J Phys* 51:287–291. <https://doi.org/10.1139/p81-059>
- Harrison AW, Vallance Jones A (1957) Measurements of the absolute intensity of the aurora and night airglow in the 0.9–2.0 μ region. *J. Sol Terr Phys, Atmos.* [https://doi.org/10.1016/0021-9169\(57\)90065-X](https://doi.org/10.1016/0021-9169(57)90065-X)
- Jones A, Vallance, Gattinger RL (1976) Quantitative spectroscopy of the aurora. IV. The spectrum of medium intensity aurora between 8800 Å and 11400 Å. *Can J Phys* 54:2128–2133. <https://doi.org/10.1139/p76-251>
- Meinel AB (1951) The auroral spectrum from 6200 to 8900 Å. *Astrophys J* 113:583. <https://doi.org/10.1086/145427>
- Nishiyama T, Taguchi M, Suzuki H et al (2021) Temporal evolutions of N_2^+ Meinel (1,2) band near 1.5 μm associated with aurora breakup and their effects on mesopause temperature estimations from OH Meinel (3,1) band. *Earth Planets Space.* <https://doi.org/10.1186/s40623-021-01360-0>
- Omholt A (1957) The red and near-infra-red auroral spectrum. *J Atmos Sol Terr Phys* 10:320–331. [https://doi.org/10.1016/0021-9169\(57\)90131-9](https://doi.org/10.1016/0021-9169(57)90131-9)
- Pallamraju D, Chakrabarti S (2005) First ground-based measurements of OI 6300 Å daytime aurora over Boston in response to the 30 October 2003 geomagnetic storm. *Geophys Res Lett* 32:L03S10. <https://doi.org/10.1029/2004GL021417>
- Pautet P-D, Taylor MJ, Pendleton WR, Zhao Y, Yuan T, Esplin R, McLain D (2014) Advanced mesospheric temperature mapper for high-latitude airglow studies. *Appl Opt* 26:5934–5943. <https://doi.org/10.1364/AO.53.005934>

- Rees D, Conde M, Steen Å, Brändström U (2001) The first daytime ground-based optical image of the aurora. *Geophys Res Lett*. <https://doi.org/10.1029/1999GL003696>
- Remick KJ, Smith RW, Lummerzheim D (2001) The significance of resonant scatter in the measurement of N_2^+ first negative 0–1 emissions during auroral activity. *J Atmos Sol Terr Phys* 63:295
- Schmidt C, Höppner K, Bittner M (2013) A ground-based spectrometer equipped with an InGaAs array for routine observations of OH(3–1) rotational temperatures in the mesopause region. *J Atmos Sol Terr Phys* 102:125–139. <https://doi.org/10.1016/j.jastp.2013.05.001>
- Shepherd SG (2014) Altitude-adjusted corrected geomagnetic coordinates: definition and functional approximations. *J Geophys Res Space Phys* 119:7501–7521. <https://doi.org/10.1002/2014JA020264>
- Singh PR, Pallamraju D, Suryawanshi P, Urmalia S (2023) Studies of atmospheric waves by ground-based observations of OH(3–1) emission and rotational temperature using PRL airglow InfraRed spectrograph (PAIRS). *J Atmos Sol Terr Phys* 244:106039. <https://doi.org/10.1016/j.jastp.2023.106039>
- Zhou X-Y, Lummerzheim D, Gladstone R, Gunapala S (2007) Feasibility of observing dayside aurora using NIR camera onboard high-altitude balloons. *Geophys Res Lett*. <https://doi.org/10.1029/2006GL028611>
- Zhou X-Y, Rafol SB, Michell RG, Hampton D, Geach C, Berk A et al (2020) Balloons in the earth's auroral science-BALBOA's modern exploration. *J Geophys Res Space Phys*. 125:e2019JA027603. <https://doi.org/10.1029/2019JA027603>

Publisher's Note

Springer Nature remains neutral with regard to jurisdictional claims in published maps and institutional affiliations.